Multi-Layer, Thin-Film Repulsive-Force Electrostatic Actuators for a 2-DoF Micro-Mirror

E. W. Schaler, L. Jiang, and R. S. Fearing
University of California, Berkeley, USA

Abstract:
This paper reports a two degree-of-freedom micro-mirror system driven by 4 flexible, multi-layer, thin-film repulsive-force electrostatic actuators (RFAs, each 13 x 19.5 mm). We demonstrate a functional multi-layer (>2-layer) RFA: it uses 4 – 8 layers for increased stroke length, has stable actuation without pull-in, has a consistent electrode pattern on each layer for ease of fabrication, separates oppositely-polarized electrodes on each layer with a polyimide substrate to prevent intra-layer shorting, and orients like-polarized electrodes on adjacent layers to prevent inter-layer shorting. We use four 4-layer RFAs (in antagonistic pairs) to drive a micro-mirror system with 35 Hz bandwidth and 8.8º / 7.6º, stable, controllable rotations about 2-DoF at up to 2000 V.

Keywords: Repulsive-Force Actuator, Electrostatic Actuator, Multi-Layer, Thin-Film

Introduction

Two complementary electrostatic actuator technologies have rapidly advanced in recent years: 2-layer MEMS repulsive-force actuators [1]–[4] and multi-layer, thin-film attractive-force actuators [5], [6]. Thin-film actuators are lightweight, cheap, and easily fabricated (compared to MEMS actuators); multi-layer actuators generate greater strokes than two-layer actuators. Repulsive-force actuators have open-loop stable operation and generate peak force at initial configurations [7]. These characteristics make a multi-layer, thin-film repulsive-force actuator (RFA) ideal for sensor platforms on meso-scale robots [8], [9].

[2], [3] demonstrate 3-DoF micro-mirrors that are fabricated via PolyMUMPs and driven by 2-layer repulsive-force actuators, with no pull-in and stable actuation over the full stroke length (±1.5º / 86 µm). Other micro-mirror systems have been produced in large arrays (±12º 1-DoF deflection) [10] and using micro-assembly (3.5º / 0.5 µm 3-DoF deflection at resonance) [11].

[6] demonstrates the feasibility of a 50-layer thin-film actuator (400 µm stroke) with unstable gap-closing actuation and a pull-in limit, while [4] models (without fabrication) a 3-layer MEMS RFA.

[7] introduces 2-layer thin-film RFAs and presented: the electrode pattern used in this paper, an out-of-plane translational actuator (511 µm stroke), and a 1-DoF rotational micro-mirror system (5.1º deflection at resonance). Other 2-layer thin-film electrostatic actuators at the meso-scale have been shown that use attractive, rather than repulsive, actuation modes, including: a linear surface-drive actuator [12], an electrostatic film motor in a 49 gram electroadhesive robot [13], and an electrostatic vibrator in a 47 mg crawling robot [14].

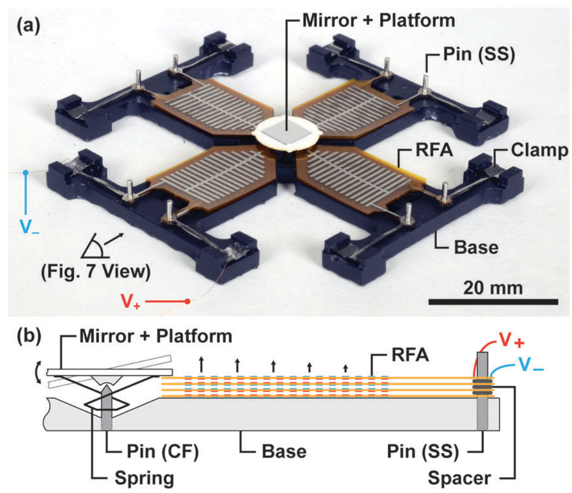

Fig. 1: Fabricated 2-DoF micro-mirror system. Image (a) and cross-section diagram (b), with 3D-printed base, four 4-layer RFAs, and spring-loaded mirror.

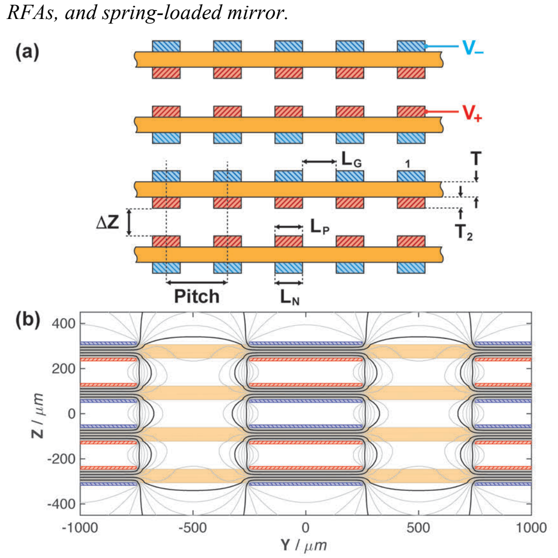

Fig. 2: Cross-section diagram (a) and electrostatic simulation (b) of the multi-layer RFA showing equipotential lines, with L_P, L_N, L_G = 500 µm, Pitch = 1000 µm, T_1 = 60 µm, T_2 = 12.5 µm. Exterior layers experience the largest electrostatic force imbalance and net repulsive forces, as seen in Fig. 5.

Fabrication

Multi-layer RFAs are easily fabricated by stacking multiple thin-film actuator layers -- we demonstrate 4 to 8-layer stacks. The fabrication process for individual layers is shown in Fig. 3. Each layer consists of two stainless steel foil electrodes (Trinity Brand Industries, 12 µm thick) adhered to each side of a polyimide (Dupont Kapton, 25 µm) substrate with thermally-activated sheet adhesive (GBC Octiva Hot Mount, 17.5 µm). The electrodes and the substrate are laser-micromachined with a UV laser (PhotoMachining Inc., 355 nm), visually aligned, and laminated to form a composite.

Fig. 4 shows an individual RFA layer and a magnified view highlighting alignment quality between electrodes on each side of the dielectric substrate (minor 35 µm misalignment is visible at the tip). The electrode dimensions in the fabricated actuator layers correspond to those defined in Fig. 2.

RFA layers are stacked to form actuators (Fig. 1, 5): pins on a 3D-printed base and spacers (100 µm) provide exact alignment constraints between layers; spring suspension (k = 2.3 N/m) from cantilevered beams and residual curvature of individual layers provides a gravity offset and restoring force. This electrode pattern is scalable to sub-100 µm features with other manufacturing processes.

Characterization

A multi-layer RFA was assembled (Fig. 5) and the actuator's free displacement dependence on number of layers was measured at two operating voltages (Fig. 6). The RFA, with 2 – 8 layers, is driven by a square-root of sinusoid signal (0 –1000 or 2000 V peak-to-peak at 0.25 Hz) for 6 cycles. The peak RFA heights each cycle are recorded by camera and measured in ImageJ. Layers are added in pairs to ensure the outermost electrodes are grounded.

RFA displacement is correlated with both number of layers and voltage: from 0.62 mm (2 layers / 1000 V) to 1.55 mm (8 layers / 2000 V) – a 2.5x increase. Displacement can thus be increased by operating at higher voltages (shown in [7]) or adding extra layers for a fixed maximum operating voltage. However, continually increasing the number of layers also increases the stack weight and therefore provides diminishing displacement returns.

RFA displacement can also be negatively affected by substrate electrostatic charging, which causes individual layers to stick together and reduces the net stack displacement. This behavior is seen in the 6-layer test with displacements of 0.30 mm at 1000 V and 1.12 mm at 2000 V (the increased repulsive force partially overcomes adhesion from residual charge). Electrostatic charging of polyimide has been reported in literature [15], [16], and minimized using an O_2 plasma etch [17].

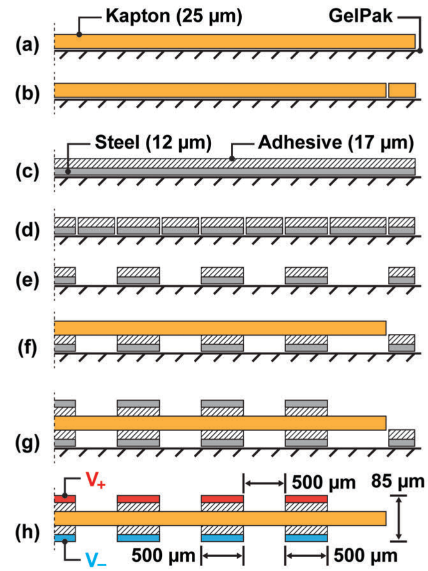

Fig. 3: Fabrication process for RFA layers. (a-b) Substrate is laser-cut from Kapton film (25 µm) secured on GelPak. (c-d) Electrodes are laser-cut from stainless steel foil (12 µm) bonded to thermally-activated sheet adhesive (17 µm) and secured on GelPak. (e) Excess foil is removed from the patterned electrodes. (f-g) Kapton substrate is visually aligned over one set of patterned electrodes, bonded (with heat), removed, flipped over, and repeated on a second set of electrodes. (h) Electrodes are powered (V_+ / V_-), with opposite sides charged differentially.

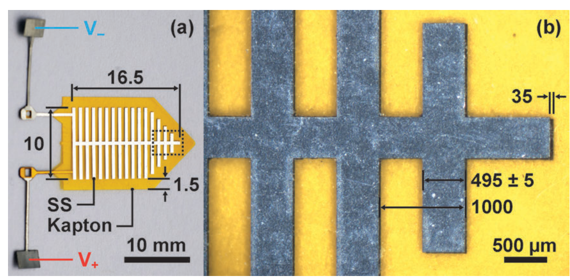

Fig. 4: RFA layer (a) with magnified view of outlined area (b).

Micro-Mirror

Fabrication

The micro-mirror assembly (Fig. 1) uses four stacks of 4-layer RFAs arranged symmetrically around a spring-loaded mirror platform. The four RFAs operate in antagonistic pairs to increase the mirror deflection about each of the two axes of rotation. The RFAs push against, but are not bonded to, the mirror platform. This creates a sliding contact point that decouples the impact of actuators operating orthogonally to one another.

The metallized glass coverslip mirror (100 µm thick) sits on a mirror platform containing a pin-and-socket joint for smooth 2-DoF pivoting with a polyimide helical spring suspension (12 µm thick) providing restoring forces. The pin is a sharpened 0.5 mm carbon-fiber rod; the socket is 3D-printed (Formlabs, Form 2).

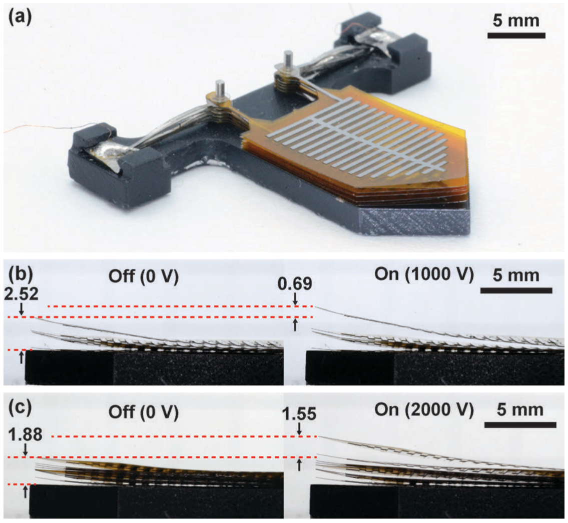

Fig. 5: *Isometric view (a) of an 8-layer RFA, and side views of a 4-layer (b) and 8-layer (c) RFA operating at 0 to 1000 / 2000 V, respectively.*

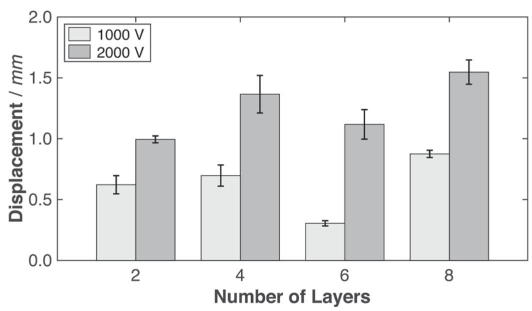

Fig. 6: *RFA displacement versus number of layers at 0 to 1000 / 2000 V, with error bars for 6 cycles of a single RFA stack. Note that static charging of the polyimide substrate reduced displacement in the 6-layer test.*

Operation

Fig. 7 shows the 2-DoF micro-mirror in operation, steering a laser beam to repeatably draw multiple patterns using open-loop control. Each actuator is driven by an individual high-voltage amplifier – Trek PZD700 for high frequency, 1000 V tests, and XP Power GP60 for low frequency, 2000 V tests – and opposing actuators are supplied inverted signals (with an offset bias of 50% peak voltage).

Fig. 8 shows the angular displacement of the mirror due to two antagonistic actuators operating on one axis of the 2-DoF micro-mirror. The actuators are driven in 100 V steps from 0 – 1000 V, with measured mirror deflections of +1.4º to -2.6º (over 5 cycles). Deflections up to 8.8º (Fig. 7) were measured when operating at 2000 V. Hysteresis is visible between forward- and back-driving the actuator – 0.27º at 500 V, the neutral position where both actuators operate at equal voltage. Discrepancy between the peak positive / negative displacement is likely due to variation in layer manufacturing, alignment, or stacking that enable one actuator to generate greater forces than the other.

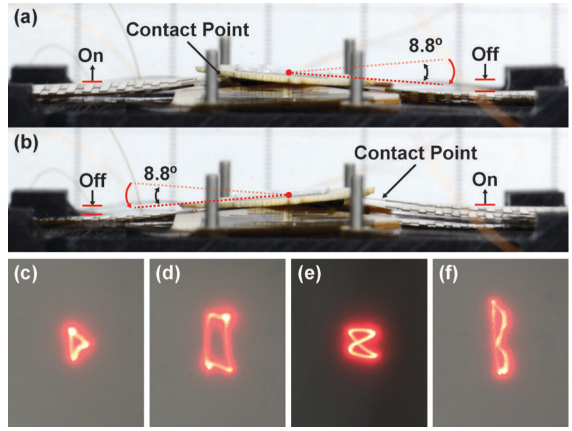

Fig. 7: *Steerable mirror deflections (a-b) along one axis at 1 Hz / 2000 V. 2-DoF laser patterns (c-f) with actuators operating at controlled waveforms between 0 – 2000 V to form (left to right): triangle, rectangle, lissajous, and 'B'.*

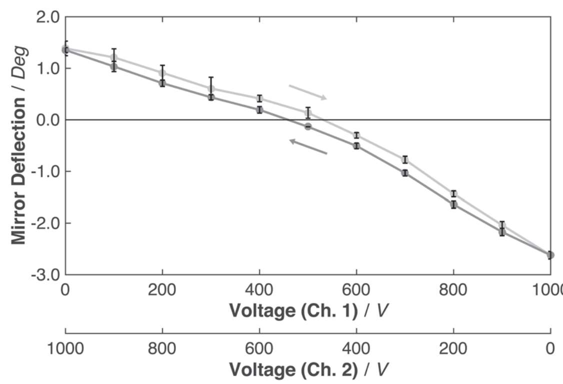

Fig. 8: *Angular displacement of mirror versus applied voltages (0 – 1000 V) of two antagonistic actuators. Average and standard deviation for 5 cycles with 0.5 sec ramp and hold in 100 V increments.*

Fig. 9 shows the frequency response for the same axis of the 2-DoF micro-mirror, with actuators now driven by 0 – 1000 V sinusoids. The mirror has a low frequency (1 Hz) net displacement of 3.8º and a bandwidth of 35 Hz (-3 dB).

The measured operating properties and peak angular displacement of the micro-mirror are presented in Table 1, along with the performance of published micro-mirror systems. Compared to existing 3-DoF systems in [2], [3], [11]: this 2-DoF system generates larger angular displacements (up to 8.8º and 7.6º at 2000 V along the two axes) and higher field strength (33 MV/m), but a lower bandwidth (35 Hz) and minimal out-of-plane translation.

Conclusions

We have demonstrated multi-layer, thin-film repulsive-force electrostatic actuators that generate greater displacements than conventional 2-layer RFAs. A simple manufacturing process using laser-cut metal foil enables rapid fabrication of many RFA layers. A 2-DoF micro-mirror system was then developed, which employs four 4-layer RFAs to stably tilt a spring-loaded mirror up to 8.8º and 7.6º

Table 1. Operational performance of this work's 2-DoF micro-mirror and comparison to existing electrostatic micro-mirror systems.

Design	Mechanical			Electrical		Performance			Source
	Process	A (*mm x mm*)	DoF (#)	V (*V*)	E (*MV/m*)	BW (*Hz*)	θ (º)	ΔZ (*μm*)	
Attractive Force	Micro-Masonry	0.9 x 0.9	3	80	2.1	1200	3.5	0.5	[11]
Repulsive Force	PolyMUMPS	3.3 x 3.3	3	200	3.8	200	±1.5	86	[2]
2-Layer RFA	Wet Etch	45 x 15	1	1000	40	16	5.1	–	[7]
		25 x 10	1	2000	40	43	–	511	[7]
4-Layer RFA	Laser	60 x 60	2	2000	33	35	8.8 / 7.6	–	This Work

A – Area **DoF** – Degrees of Freedom **V** – Voltage **E** – Electric Field Strength **BW** – Bandwidth **θ** – Angular Displacement **ΔZ** – Normal Displacement

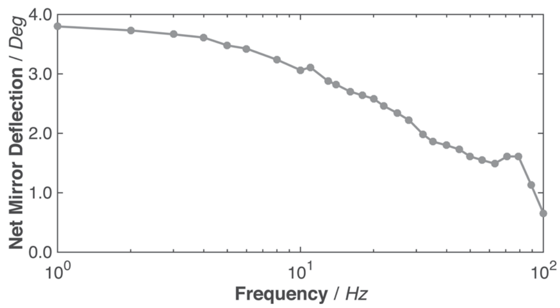

Fig. 9: *Angular displacement of mirror (net) versus operating frequency, for actuators operating with an applied sinusoidal voltage at 0 – 1000 V.*

on its two axes with a 35 Hz bandwidth. Prior MEMS devices were limited to angular deflections of ±1.5º [2] (stable) and 3.5º [11] (unstable), albeit with higher bandwidth.

Future work will reduce the RFA layer size for a more compact system, explore linear (as opposed to cantilever) suspensions for greater angular deflection, and add capacitive sensing for closed-loop control of mirror position.

Acknowledgements

We thank M. Hettick and A. Javey for use of a plasma etcher, to test protocols for minimizing static charging of the polyimide substrates.

Funding was provided in part by the National Science Foundation via grant CMMI-1427096.

References

[1] W. C. Tang, M. G. Lim, and R. T. Howe, "Electrostatic comb drive levitation and control method," *J. Microelectromech. Syst.* 1, 4 (1992), 170–178.

[2] S. He, R. Ben Mrad, and J. Chong, "Repulsive-force out-of-plane large stroke translation micro electrostatic actuator," *J. Micromech. Microeng.* 21, 7 (2011), 75002.

[3] S. Towfighian, S. He, and R. Ben Mrad, "A low voltage electrostatic micro actuator for large out-of-plane displacement," in *ASME IDETC/CIE* (2014), 1–7.

[4] S. He and R. Ben Mrad, "Performance assessment of a multi-level repulsive-force out-of-plane microelectrostatic actuator," *Can. J. Elect. Comput. Eng.* 31, 2 (2006), 71–75.

[5] K. Minami, S. Kawamura, and M. Esashi, "Fabrication of distributed electrostatic micro actuator (DEMA)," *J. Microelectromech. Syst.* 2, 3 (1993), 121–127.

[6] M. Ito and K. Saneyoshi, "Development of large-scale stacked-type electrostatic actuators for use as artificial muscles," *Adv. Robot.*, 1864 (2014), 1–9.

[7] E. W. Schaler, T. I. Zohdi, and R. S. Fearing, "Thin-film repulsive-force electrostatic actuators," *Sensors Actuators A Phys.*, 270 (2018), 252–261.

[8] D. W. Haldane, C. Casarez, J. Karras, J. Lee, C. Li, A. Pullin, E. Schaler, D. Yun, A. Javey, and R. S. Fearing, "Integrated manufacture of exoskeleton and sensing for folded millirobots," *J. Mech. Robot.* 7, 2 (2015), 19.

[9] A. Buchan, "Towards Cooperative SLAM for Low-Cost Biomimetic Robots," EECS Department, University of California, Berkeley (2017).

[10] Texas Instruments, "DMD 101: Introduction to Digital Micromirror Device (DMD)," (2013).

[11] Z. Yang, B. Jeong, A. Vakakis, and S. Kim, "A tip-tilt-piston micromirror with an elastomeric universal joint fabricated via micromasonry," *J. Microelectro-mech. Syst.* 24, 2 (2015), 262–264.

[12] T. Niino, S. Egawa, and T. Higuchi, "High-power and high-efficiency electrostatic actuator," in *IEEE MEMS* (1993), 236–241.

[13] H. Wang, A. Yamamoto, and T. Higuchi, "Electrostatic-motor-driven electroadhesive robot," in *IEEE/RSJ IROS* (2012), 914.

[14] M. Qi, Y. Zhu, Z. Liu, X. Zhang, X. Yan, and L. Lin, "A fast-moving electrostatic crawling insect," in *MEMS* (2017), 761-764.

[15] M. J. Duck, "Surface charging and its prevention," in *The Behavior of Systems in the Space Environment*, R. N. DeWitt, D. Duston, and A. K. Hyder, Eds. Dordrecht: Springer Netherlands (1993), 867–872.

[16] D. Verdin, "Electrostatic discharging behaviour of Kapton irradiated with electrons," *Spacecr. Charg. Technol.* (1981), 96–114.

[17] J. H. Lee and H. C. Jeong, "Removal of static electricity on polyimide film surface by O2 or Ar cold plasma etching," *Fibers Polym.* 5, 2 (2004), 151–155.